FRACTURE (ULTIMATE STRENGTH) ANALYSES OF ASPHALT PAVEMENT LAYERS RESULTING FROM TRAFFIC LOADING

Y. M. Salam, American University of Beirut, Lebanon; and
C. L. Monismith, University of California, Berkeley

This paper presents analyses of fractures occurring in asphalt pavement structures due to excessive single-wheel loads and to braking tractions applied at the pavement surface. Specific solutions using a plane-stress finite-element idealization wherein nonlinear material responses and bond effects at layer interfaces could be considered are presented for cracking in an asphalt concrete bridge deck surfacing, for development of cracking in an asphalt concrete layer over a cement-treated base that was cracked due to load, and for cracking resulting from tractions imposed on an airfield pavement by a braking aircraft. The bridge deck surfacing incorporated two different support conditions, rigid and flexible, and two sets of material characteristics. For the flexible-support condition, the bituminous surfacing failed by compression and the stiffer material ruptured at a lower load; for the rigid-support condition, the stiffer material failed in tension at a higher load than the low-modulus material, which exhibited a compressive failure. The effect of low bond strength on this latter condition was to shift the failure condition from compression to a mixed mode. The ultimate strength of a pavement containing cement-treated base was determined by tensile fracture of the cement-treated base followed by subsequent cracking of the upper portion of the asphalt concrete layer. Braking tractions in a runway pavement resulted in lowering the total load to failure by increasing the tensile stresses at the heel of the loaded area. A weak interface also resulted in a further decrease of the total fracture loads.

•ASPHALT pavements can exhibit cracking that may result from both traffic-load- and non-traffic-associated causes. Table 1 gives some potential causes of fracture of this type. Cracking resulting from fatigue has received considerable attention in recent years (1) as has cracking resulting from thermal stresses associated with low temperatures (1). Some methodology has also been presented to illustrate procedures whereby cracking due to shrinkage in cement-treated materials can be estimated (2, 3).

Little information has been presented in the area of traffic-load-associated cracking due to excessive single loads or slippage distress resulting from braking tractions. This, perhaps, has been due in part to the limited nature of the initial distress resulting from these causes (1). It may also be due to the fact that no suitable method of analysis exists to examine the ultimate strength capabilities for realistic (three-dimensional) situations.

This paper will present an initial attempt of the analysis of such problems in the pavement area, the format for which is shown in Figure 1, and will examine specific solutions for cracking in an asphalt concrete bridge deck surfacing, development of cracking in an asphalt concrete layer over a cement-treated base that was cracked due to load, and cracking resulting from tractions imposed on an airfield pavement by a

Publication of this paper sponsored by Committee on Theory of Pavement Design.

braking aircraft. It should be noted that the analysis will be restricted to plane stress conditions but permits the idealization of nonlinearity of material response and bond effects at layer interfaces.

METHOD OF ANALYSIS

The method of analysis, the results of which are presented here, provides a format for studying the effect of progressive loading on pavement systems with emphasis on ultimate behavior. This type of loading results, at the higher levels of load, in decreased structural stiffness resulting from material nonlinearity and cracking and fracturing of individual elements resulting from limiting tension or compression strength criteria. As will be seen, fracturing, stresses, and displacements can successively be predicted.

When asphalt concrete is subjected to large stresses (near the ultimate strength), a nonlinear constitutive law is observed for a wide range of temperatures and loading times (7). Nonlinearity may also result because of local characteristics (e.g., voids) that act as stress raisers leading to local failures that amplify the global response into the nonlinear range.

When a pavement is monotonically loaded, a set of displacements will occur within and between the different layers. The force-displacement relations are determined by the element stiffnesses (of the discrete system), the internal connectivity between elements, and the external boundary conditions. As the load is increased, changes in element stiffnesses occur because of decreased material modulus at higher stresses or propagation of existing starter cracks. Such cracking results in the redefinition of the pavement being analyzed because a different internal stress distribution results and reorientation of the principal stresses occurs. This process is affected to varying degrees by differences in layer material response and prior loading history.

A finite-element idealization of bond-slip behavior has been suggested by Ngo and Scordelis (4) in conjunction with reinforced concrete. The interface is idealized by a series of linkage elements each containing two springs, one acting parallel to the direction of slip and the other perpendicular to it. The two springs may be uncoupled so that their behavior could be independent, or they could be made to interact if considered appropriate. This concept was further used by Nilson (5) for the finite-element analysis of reinforced concrete. The method employed here used the procedure developed by Franklin (6), who combined bond-slip behavior with material nonlinearity to analyze reinforced concrete frames and panels under plane stress states. The procedure is essentially an incremental iterative solution that provides for the cracking of individual material elements, with stress redistribution in the surrounding elements by iteration. Within each load increment, a number of iterations are performed to improve the stiffness value for that increment, with the initial stiffness derived from the previous increment, and an initial stiffness introduced to start the analysis.

The incremental procedure provides the bounds that isolate and identify successive failures. The external load is kept constant, whereas the solution is iterated to establish equilibrium of the system within a specified increment.

The fracturing of an element results in partial or total loss of the element stiffness. In addition, it will cease to carry part or all of the imposed loads, with the corresponding fraction of the released strain energy redistributed into the surrounding elements. This process of unloading may be explained as follows: Suppose that an element fails at increment i - 1 the total element nodal forces are $\{S_1\}$ and the total nodal deflections are $\{v_1\}$, with a corresponding element sitffness $[k_1]$. When the element fractures, a new element stiffness $[k_2]$ results with a corresponding release of forces at the nodes. Thus, for fixed nodes, equilibrium is achieved for the fractured element at a new set of nodal forces $\{S_2\}$ given by $\{S_2\} = [k_2]\{v_1\}$ with $\{S_f\} = \{S_1\} - [k_2]\{v_1\}$. $\{S_f\}$ is the element fracture release force accompanying a total or partial release of strain energy depending on whether or not $[k_2]$ is zero. Combining the forces $\{S_f\}$, the self-equilibrating vector of node fracture forces, the increment equation takes the form: $\{R\} + \{R_f\} = [K]\{r\}$, with $\{R_f\}$ appearing as an additional external loading. The iterations are performed until convergence occurs. Within this

context, fracture is considered as a factor that disturbs the rate of convergence of the iteration process. The system stiffness is allowed to adjust before the following load increment is applied, and the process is terminated when extensive structural damage occurs.

Because the program required extensive computer (CDC 6400) time (approximately 3 min per run), a relatively small-sized finite-element mesh was utilized. The problems investigated showed that the accuracy of the stress distribution predictions dropped with excessive cracking. (After failure of the first few elements had occurred, the rate of convergence of stiffnesses dropped, and the accuracy of the stresses predicted in the remaining intact elements decreased.)

The material properties required for the analysis were obtained from a laboratory study (7) and included stress-strain characteristics as well as ultimate tensile and compressive strengths.[1] Stress and strain curves were divided into eight linear portions for input to the computer program. Element fracturing, stress patterns, and displacements were determined in each of the problems investigated.

EXAMPLES OF THE STRUCTURAL ANALYSIS

Because of the complexity of the analysis used to obtain the results presented in this section, the examples have been selected on the basis of simplicity, computer time efficiency, and practicality as permitted by the plane stress state. Exact duplication of actual conditions is not possible at this time, and details that might have obscured the procedure or complicated the analysis were excluded.

The examples have been chosen to permit the comparison of pavement response under different boundary conditions and with different material properties. However, it must be recognized that the loads at fracture that have been estimated should be examined more on a comparative basis than in the absolute sense.

Cases examined in the computations include the following:

1. Asphalt concrete bridge deck surfacing with flexible support and rigid support (temperature of asphalt concrete at 68 and 40 F),
2. Asphalt concrete over a cement-treated base, and
3. Thick asphalt concrete runway pavement with vertical load only and with vertical load combined with braking traction (fixed bond at interface between pavement and underlying layer and weak interface).

Asphalt Concrete Bridge Deck Surfacing

Preliminary analyses indicated that the response of the asphalt concrete surfacing is a function of the rigidity of the supporting girder, with a flexible girder having the potential to induce a stress pattern differing markedly from that resulting from a rigid support. Both conditions were investigated with the same finite-element mesh but with differing boundary conditions.

Figure 2 shows the finite-element idealization representing a 5-in. thick half-section of a 14-in. girder with a 4-in. asphalt concrete cover. This section width was chosen because of its compatibility with plane stress states. A rigid support was obtained with roller A in place, whereas the flexible condition was obtained by deleting roller A. The girder was assumed to be linear elastic with a modulus of 30×10^6 psi (representative of structural steel). Linearized stress-strain characteristics of the asphalt concrete are shown in Figure 3. In addition, the biaxial strength envelopes shown in Figure 4 were used as failure criteria and were incorporated in the program. Characteristics of the bond between asphalt concrete and steel were not available. Accordingly, the interface was assigned a constant stiffness modulus equal to half the initial stiffness of the asphalt concrete, and bond effects were analyzed for the rigid support condition at 68 F.

[1] The original manuscript of this paper included Appendix A, Characteristics of Asphalt Concrete, and Appendix B, Incremental Iteration Method. The appendixes are available in Xerox form at cost of reproduction and handling from the Highway Research Board. When ordering, refer to XS-47, Highway Research Record 466.

Table 1. Categories of fracture in asphalt pavements.

General Cause	Specific Causative Factor	Visual Manifestation of Distress
Traffic-load associated	Repetitive traffic loading	Fatigue
	Horizontal forces, e.g., braking loads at pavement surface	Slippage
	Single or comparatively few excessive loads	Longitudinal or transverse cracks or both
Non-traffic associated	Thermal changes	Transverse cracks (relatively uniformly spaced)
	Shrinkage of treated materials (e.g., of cement-treated base)	Transverse cracks (relatively uniformly spaced)
	Moisture changes	Transverse cracks (relatively uniformly spaced)

Note: Table contains only a partial listing.

Figure 1. Fracture subsystem.

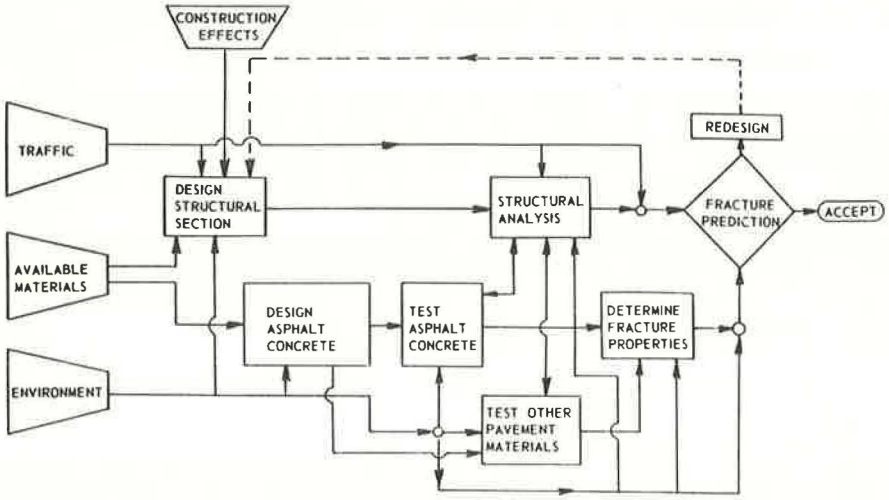

Figure 2. Finite-element idealization of bridge deck.

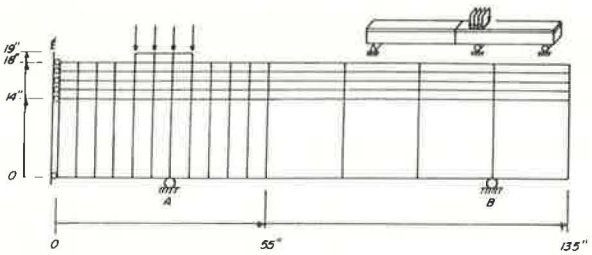

Figure 3. Asphalt concrete mix stress and strain data.

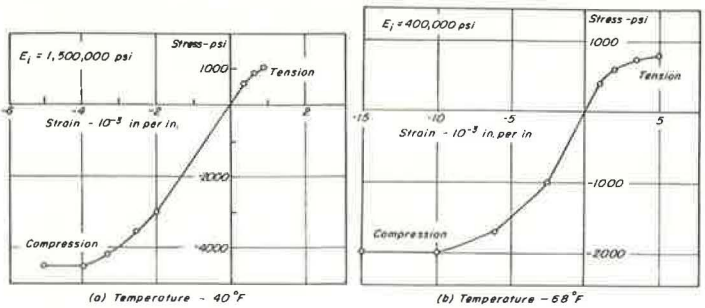

Load was applied to the surfacing through a loading strip 15 in. in length over four nodal points (Fig. 2). Braking forces were simulated by applying a horizontal load that was made equal to one-half of the vertical load. For a particular case, large load increments were first used to determine approximately the ultimate value; the problem was then rerun using smaller increments near the ultimate load.

Flexible Support—Results of the analyses for this condition are shown in Figures 5 through 7 for a mix temperature of 40 F and in Figures 8 through 10 for a mix temperature of 68 F. Generally, the response of the asphalt concrete is determined by the deflection of the supporting girder, and large compressive stresses are induced throughout the depth of the asphalt-bound layer. These stresses are increased in the region ahead of the loaded area because of the horizontal component of the load.

For the 40 F condition, Figure 5 shows the variation in horizontal strains and vertical deflections at the surface of the asphalt concrete prior to failure (load of 80 kip) along the girder. Figure 6 shows the distribution of the minimum stresses (maximum compressive stress for the individual elements) at the onset of fracture.

Figure 7 shows the sequence of fracture, which is indicated by the numbers 1, 2, 3, and 4 in the critical area when the total vertical load reached 84 kip. As would be anticipated (Fig. 6), the first elements to fail were those immediately ahead of the load, followed by those at the heel. At this temperature, distress occurs in compression due to the high compressive strains, and the failure area appears reasonably well distributed under the loaded area.

At 68 F, because the asphalt concrete is less stiff, larger deflections are tolerated (Fig. 8). At a load of 120 kip, at which failure was imminent, similar trends in stresses to those observed at 40 F were obtained (Fig. 9). In this instance, the stress at the toe of the load is almost twice that at the heel. As seen in Figure 10, failure occurs more extensively in this area at a load of about 140 kip.

Rigid Support—The same finite-element mesh as for the flexible condition was used to solve this problem. Figures 11 through 13 show the results of the analysis for a mix temperature of 40 F, and Figures 14 through 16 show the results for 68 F. In addition to the cases illustrated in these figures, a case was analyzed, as noted earlier, to study the effect of bonding between the asphalt concrete and the supporting member by assigning a stiffness at the interface equal to one-half that of the asphalt concrete. Results of this analysis for a mix temperature of 68 F are shown in Figures 17 and 18.

For the 40 F case (Fig. 11), the horizontal strains are tensile at the rear of the load and compressive in front of it. For this situation, the tensile condition is critical.

For a load of 160 kip, Figure 12 shows minimum and maximum stress distributions in the asphalt concrete beneath the loaded plate. The maximum compressive stress was approximately 2,100 psi, whereas the maximum tensile stress was about 850 psi. If these conditions were plotted in Figure 4, it would be noted that the tensile stress is more critical.

The sequence of fracture under a load of 200 kip is shown in Figure 13 and, as noted previously, is initiated on the tensile side. This figure also shows the directions of the maximum and minimum stresses prior to failure and illustrates the effect of the horizontal load on the orientation of stresses.

At 68 F, the compression effects are more pronounced because the ratio of compression to tensile strength is lower than at 40 F. Figure 14 shows the distribution of strains and deflections for a load of 136 kip (onset of fracture), and Figure 15 shows the corresponding stress distributions. The sequence of fracture at 140 kip is shown in Figure 16, indicating the stronger influence of compression in contributing to distress (as compared to 40 F, Fig. 13).

The influence of bonding between the asphalt concrete and the support is shown in Figures 17 and 18. At the onset of cracking, the stress distribution was similar to the case of fixed bond, but failure occurred at a lower load (112 kip). However, the cracking appeared to shift slightly to the tension side as shown in Figure 17. The difference between the fixed bond and the weak interface is shown more clearly in Figure 18 where the horizontal strain 1 in. above the interface is plotted with the applied load.

Figure 4. Asphalt concrete mix biaxial strength envelopes.

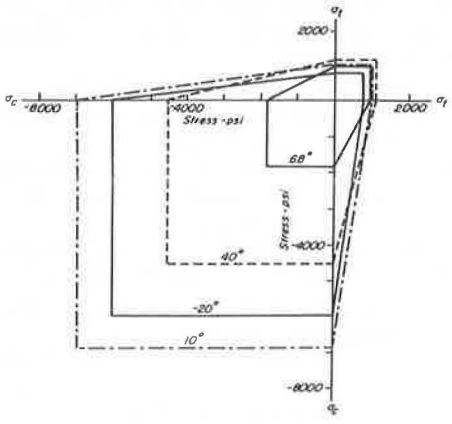

Figure 5. Horizontal strains and vertical deflections at surface of asphalt concrete cover, flexible support (40 F).

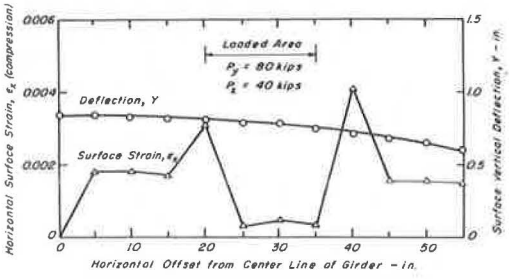

Figure 6. Distribution of maximum compressive stresses in asphalt concrete surfacing, flexible support (40 F).

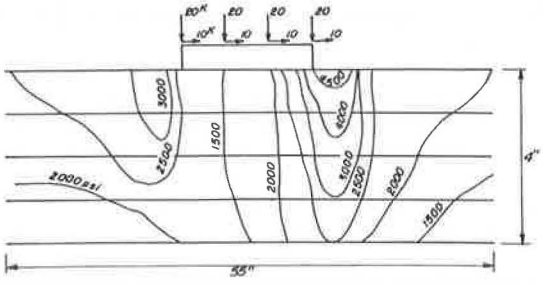

Figure 7. Fracture sequence in asphalt concrete surfacing, flexible support (40 F).

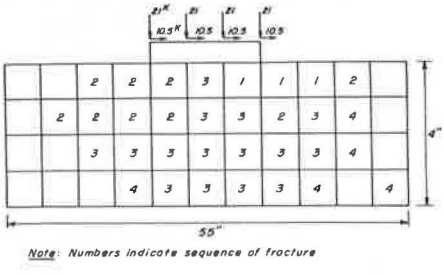

Figure 8. Horizontal strains and vertical deflections at surface of asphalt concrete cover, flexible support (68 F).

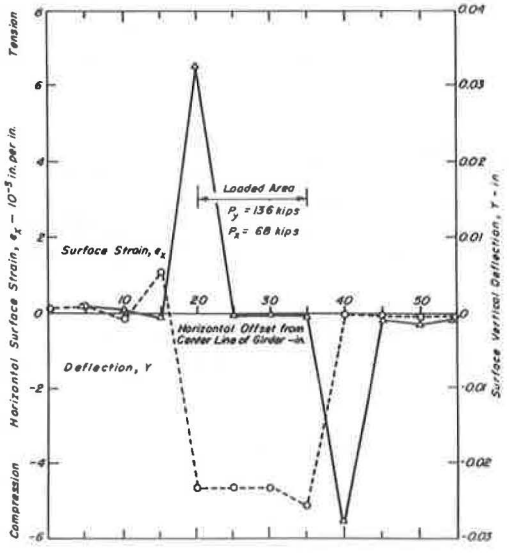

Figure 9. Distribution of maximum compressive stresses in asphalt concrete surfacing, flexible support (68 F).

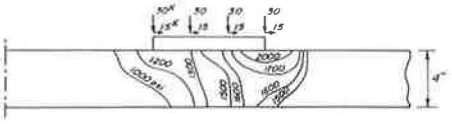

Figure 10. Fracture sequence in asphalt concrete surfacing, flexible support (68 F).

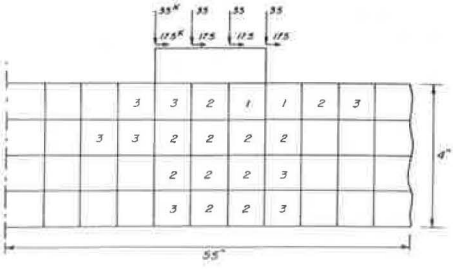

Figure 11. Horizontal strains and vertical deflections at surface of asphalt concrete cover, rigid support (40 F).

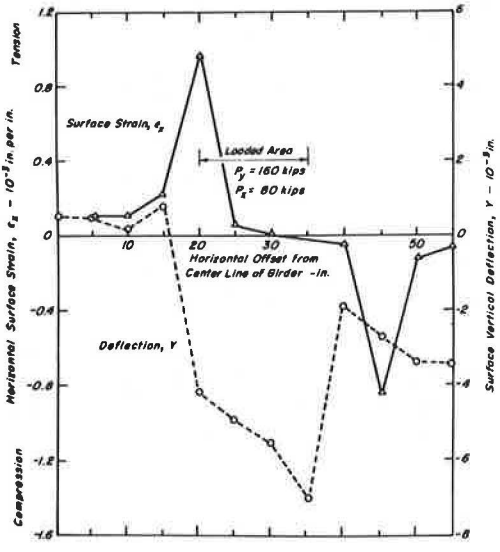

Figure 12. Distribution of minimum and maximum stresses in asphalt concrete surfacing, rigid support (40 F).

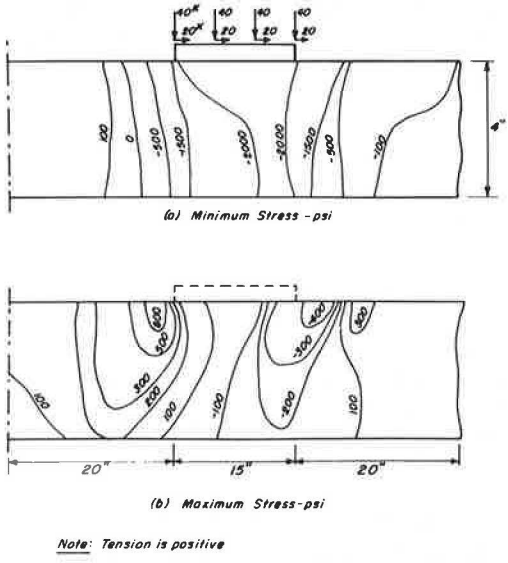

Figure 13. Sequence of fracture and orientation of maximum and minimum stresses prior to fracture in asphalt concrete surfacing, rigid support (40 F).

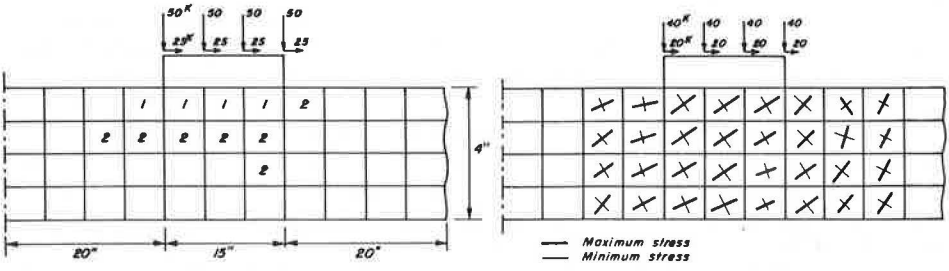

Figure 14. Horizontal strains and vertical deflections at surface of asphalt concrete cover, rigid support (68 F).

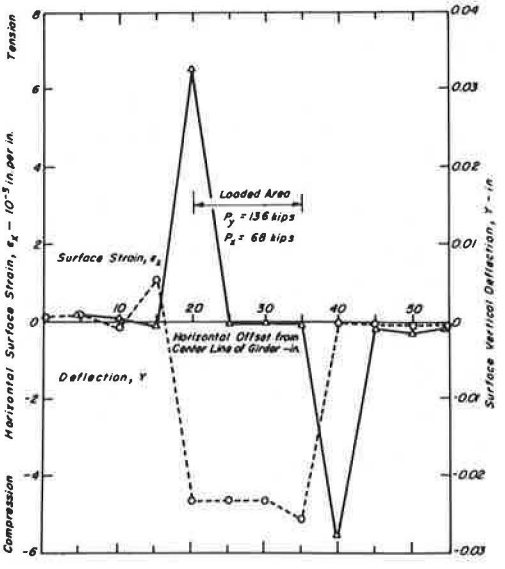

Summary and Comment

Effects of boundary conditions on the ultimate load-carrying capabilities of an asphalt concrete layer on a bridge deck may be summarized as follows:

Condition	Load to Failure (kip)	Mode of Failure
Flexible support		
40 F	84	Compression
68 F	120	Compression
Rigid support		
40 F	200	Tensile
68 F	140	Compression
68 F (weak interface)	112	Mixed

For the flexible support conditions, the maximum deflections, Y, were approximately 0.85 in. (Fig. 5) and 1.4 in. (Fig. 8). These values are in the range that might be expected in practice, e.g., allowable maximum of 1.5 in. for steel bridges of 100-ft spans ($^1/_{800}$ of the span length) and 0.75 in. for concrete bridges with 50-ft spans. For the rigid case, the deflection, Y, is very small (Figs. 11 and 14).

Asphalt Concrete Layer Over a Cement-Treated Base

The analysis described in this section is restricted to studying fracture progression in an asphalt concrete surface as the result of cracking of the underlying cement-treated base because of excessive loading.

The finite-element mesh used is shown in Figure 19. For this analysis, the pavement has been idealized as a composite beam 5 in. in width consisting of an 8-in. thick asphalt concrete layer and a 10-in. thick cement-treated base symmetrically located on a subgrade strip 10 in. in width. (This dimension was chosen to impart stability to the foundation layer relative to its extent in the vertical plane and its low modulus.) Load was applied at two nodal points of a 10-in. long plate (Fig. 19).

Stress-strain characteristics in tension and compression at 68 F for the asphalt concrete are the same as those used in the previous example (Fig. 3b). The stress-strain relation for the cement-treated base was obtained from data developed by Pretorius (2) (Fig. 20). An elastic modulus of 10,000 psi was used for the subgrade.

Variation of the vertical deflection at the surface of the pavement with horizontal offset measured from the centerline of the beam is shown in Figure 21 for a load of 20 kip (onset of cracking). Fracture occurred at a load of 22 kip in the sequence shown in Figure 22. The first element to crack was element 1 of the cement-treated base. Further cracking in the cement-treated base occurred adjacent to element 1 together with tensile fracture at the upper layers of the asphalt concrete surface. Further failures took place subsequently in the bottom layers.

This type of cracking has also been reported by Pretorius (2) based on the analysis of stresses in the pavement, idealized in the form of a prismatic space, after the cement-treated base had cracked due to shrinkage stresses.

Cracking Due to Braking Stresses Applied at Pavement Surface

This analysis is concerned with the development of stresses in the asphalt concrete layer due to braking stresses (representative of an aircraft loading) applied at the pavement surface. A friction factor between tire and pavement of 0.5 has been assumed, and both horizontal and vertical components of load have been applied at the same time.

The finite-element representation is shown in Figure 23, the pavement consisting of an asphalt concrete beam 5 in. wide and 20 in. deep on a subgrade strip 10 in. wide. As seen in the figure, the load (representative of a heavy aircraft load) was applied through an elastic plate 20 in. in length. Properties of the asphalt concrete were those shown in Figure 3a (a temperature of 40 F was assumed for this example); a subgrade stiffness of 10,000 psi was utilized.

Figure 15. Distribution of minimum and maximum stresses in asphalt concrete surfacing, rigid support (68 F).

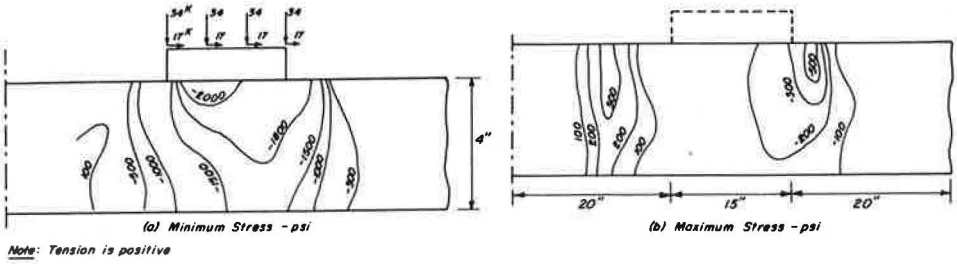

Figure 16. Sequence of fracture and orientation of maximum and minimum stresses prior to fracture in asphalt concrete surfacing, rigid support (68 F).

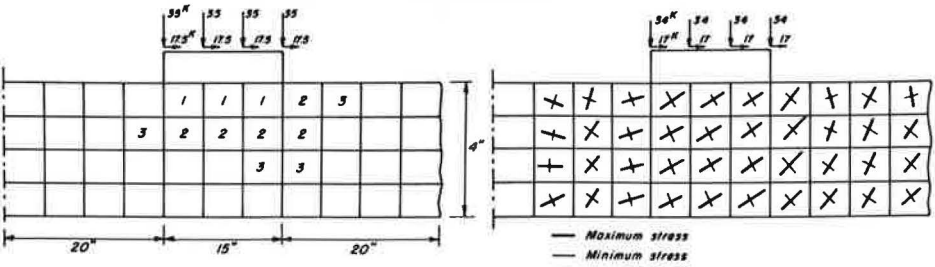

Figure 17. Sequence of fracture in asphalt concrete surfacing with weak interface, rigid support (68 F).

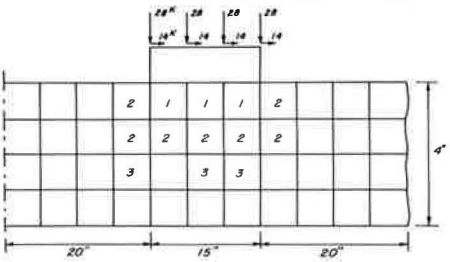

Figure 18. Effect of weak interface on strength of asphalt concrete surfacing, rigid support (68 F).

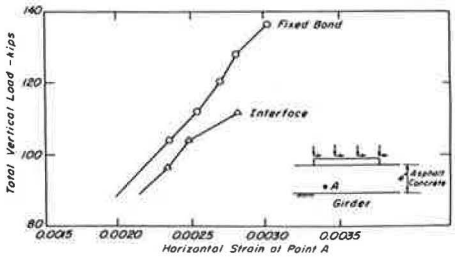

Figure 19. Finite-element mesh for pavement section with cement-treated base.

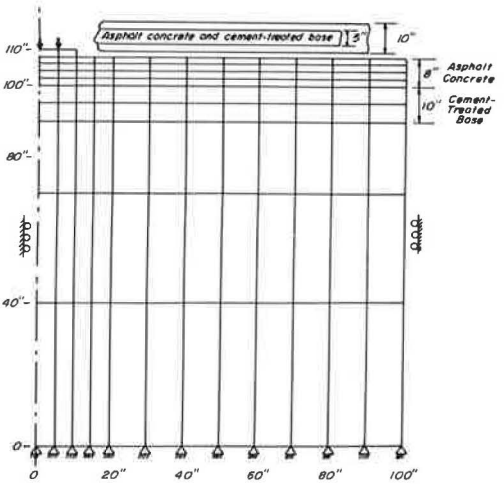

Figure 20. Stress-strain data for cement-treated base.

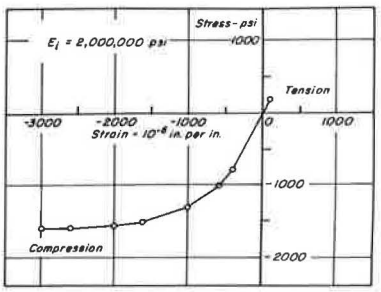

Figure 21. Variation of surface deflection with distance from centerline of load.

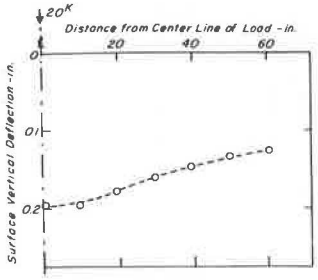

Figure 22. Sequence of fracture in pavement containing cement-treated base.

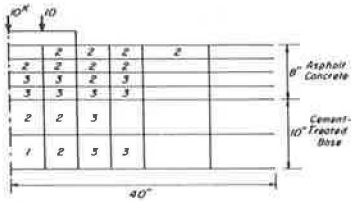

Figure 23. Finite-element idealization of runway pavement for braking tractions.

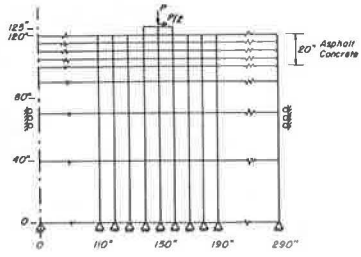

Figure 24. Influence of 44-kip vertical load applied to surface of 20-in. thick asphalt concrete layer (40 F).

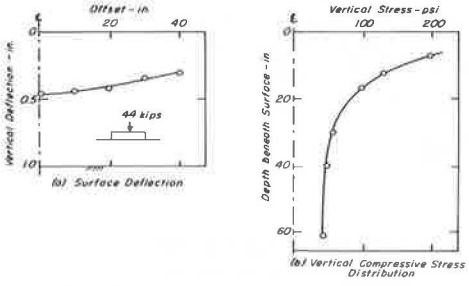

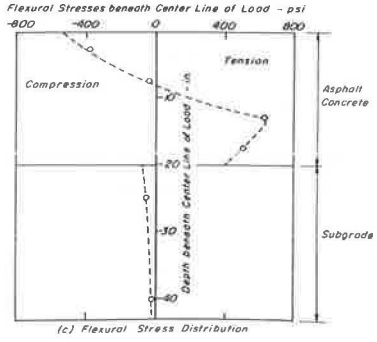

Figure 25. Fracture sequence in 20-in. asphalt concrete runway pavement for vertical loads (40 F).

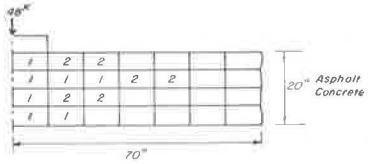

Figure 26. Horizontal stress distribution in 20-in. thick asphalt concrete runway pavement under braking tractions prior to cracking (40 F).

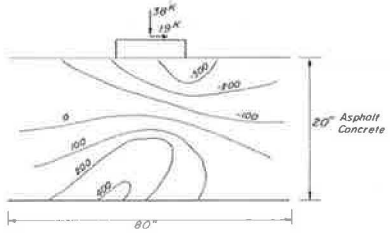

Figure 27. Fracture sequence in 20-in. thick asphalt runway pavement subjected to braking tractions.

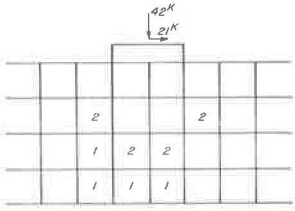

Figure 28. Variation of the horizontal strain at point A with applied loads for fixed-bond and weak-interface conditions.

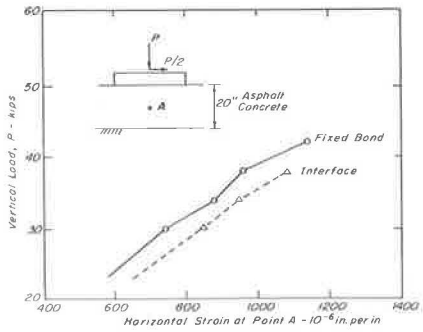

An analysis was first accomplished for only the vertical loading condition. Figure 24 shows the results of this analysis: surface deflection (Fig. 24a), vertical stress as a function of depth (Fig. 24b), and distribution of flexural stresses with depth (Fig. 24c).

The truncation of the tensile stresses at the bottom of the asphalt concrete might have resulted from forces released by those elements due to crack initiation. Figure 25 shows the sequence of cracking that occurred symmetrically over the full depth of the section at a total load of 48 kip.

Stress estimates including the effect of horizontal tractions are shown in Figure 26. In this figure, the horizontal (flexural) stress distribution for a vertical load of 38 kip is shown; it can be seen that the distortion of the flexural stress field has resulted from the compressive stresses at the toe of the load plate and tensile stresses at the heel. Fracture occurred in tension below the heel at a load of 42 kip (Fig. 27).

The effect of a weak interface between the asphalt concrete pavement and the subgrade was analyzed. The stress distribution and the fracture sequence were similar to the fixed bond condition, but the fracture load was slightly lowered. Horizontal strains were higher in the case of the weak interface as shown in Figure 28.

SUMMARY

In this paper, methodology for performing ultimate strength analyses for certain pavement structures has been briefly summarized. For simplicity, only plane stress conditions have been utilized.

The procedure involves an incremental loading pattern with solution iteration within each load increment. Predictions of cracking, stress distributions, and displacements were obtained for three examples.

The bridge deck surfacing incorporated two different support conditions, rigid and flexible, and two sets of material characteristics. For the flexible-support condition, the asphalt surfacing failed by compression and the stiffer material ruptured at a lower load. In the rigid-support condition, the stiffer material failed in tension at a higher load than the low-modulus material, which exhibited a compressive failure. The effect of low bond strength on this latter condition was to shift the failure condition from compression to a mixed mode.

The ultimate strength of a pavement containing cement-treated base was determined by tensile fracture of the cement-treated base followed by subsequent cracking of the upper portion of the asphalt concrete layer.

Braking tractions in a runway pavement resulted in lowering the total load to failure by increasing the tensile stresses at the heel of the loaded area. A weak interface also resulted in a further decrease of the total fracture loads.

Although the analyses presented here are restricted to plane stress conditions and can only be considered as a pilot study, they illustrate how critical areas can be defined in pavement structures (for example, the bridge deck pavement wherein two boundary conditions and two sets of materials were analyzed) and may thus provide some insight to techniques to minimize load associated fracture.

ACKNOWLEDGMENTS

The investigation was supported by the Federal Highway Administration. This agency has not reviewed the research findings.

REFERENCES

1. Structural Design of Asphalt Concrete Pavement Systems. HRB Spec. Rept. 126, 1971.
2. Pretorius, P. C. Design Considerations for Pavements Containing Soil-Cement Bases. Univ. of California, Berkeley, PhD dissertation, 1970.
3. George, K. P. Shrinkage Characteristics of Soil-Cement Mixtures. Highway Research Record 255, 1968, pp. 42-58.
4. Ngo, D., and Scordelis, A. C. Finite Element Analysis of Reinforced Concrete Beams. Jour. of American Concrete Institute, Vol. 64, March 1967.

5. Nilson, A. H. Finite Element Analysis of Reinforced Concrete. Univ. of California, Berkeley, PhD thesis, 1967.
6. Franklin, H. A. Nonlinear Analysis of Reinforced Concrete Frames and Panels. Univ. of California, Berkeley, PhD thesis, 1970.
7. Salam, Y. M. Characterization of Deformation and Fracture of Asphalt Concrete. Univ. of California, Berkeley, PhD dissertation, 1971.